



Cite this: *RSC Adv.*, 2020, **10**, 18543

Received 16th March 2020  
 Accepted 6th May 2020

DOI: 10.1039/d0ra02420a  
[rsc.li/rsc-advances](http://rsc.li/rsc-advances)

## Atomic and electronic structures of charge-doping VO<sub>2</sub>: first-principles calculations

Lanli Chen, <sup>ab</sup> Yuanyuan Cui, <sup>b</sup> Hongjie Luo <sup>b</sup> and Yanfeng Gao, <sup>\*bc</sup>

The atomic and electronic structures of charge-doping VO<sub>2</sub> are investigated by using first-principles calculations. Hole doping is more conducive to stabilizing the structure of VO<sub>2</sub> than electron doping. The controllable phase transition temperature is coupled with changes in atomic and electronic structures. With the increase in hole density, the V–V chains and twisting angle experience a dramatic change, and the band gap (0.69–0 eV) is rapidly reduced due to orbital switching between the d<sub>x<sup>2</sup>-y<sup>2</sup></sub> and d<sub>z<sup>2</sup></sub>/d<sub>yz</sub> orbitals. However, as the electron density increases, the band gap (0.69–0.502 eV) narrows slightly, while the V–O bond lengths significantly increase. The current results provide up a variable way to tune the VO<sub>2</sub> phase transition temperature through charge-doping.

### 1. Introduction

Vanadium dioxide (VO<sub>2</sub>) is an attractive thermochromic material due to its reversible metal–insulator transition (MIT) from a high-temperature rutile phase (R) to a low-temperature monoclinic phase (M) at a phase transition temperature (*T<sub>c</sub>*) of about 68 °C. Across the MIT, VO<sub>2</sub> exhibits a dramatic change in its electrical and optical properties.<sup>1</sup> Therefore, VO<sub>2</sub> is not only attracting wide scientific interest but also has great technological applications in optoelectronic devices,<sup>2,3</sup> sensors,<sup>4</sup> and smart windows.<sup>5–7</sup>

Given the diverse potential applications for VO<sub>2</sub>, modulation of the phase transition behavior and decreasing the *T<sub>c</sub>* close to room temperature are the main hottest topics in VO<sub>2</sub> researches. The control of phase transition in VO<sub>2</sub> was successfully implemented with multiple ways including doping,<sup>8,9</sup> point defects,<sup>10,11</sup> external strain,<sup>12</sup> electric fields,<sup>13</sup> and surface and interface engineering.<sup>14</sup> In most of these modulations, doping was proposed to play a strong role in mediating the phase transition temperature of VO<sub>2</sub>. Recently, it is reported that charge-doping could effectively decrease the *T<sub>c</sub>* of VO<sub>2</sub>. What's the effect of the two types of charge injection, *i.e.* the hole or electron injection, on the tuning the MIT of VO<sub>2</sub>? For example, Zhang *et al.*<sup>15</sup> found that the reduction of the *T<sub>c</sub>* is essentially ascribed to the charge injection as the dopants by the first-principles calculations. The surface adsorption of F<sub>4</sub>TCNQ molecules assists the phase transition of VO<sub>2</sub> film due to the surface charge transfer.<sup>16</sup> Substitution N-doping or interstitial N-doping in VO<sub>2</sub> allows for a significant reduction in the phase transition temperature from 80.0 to 62.9 °C.<sup>17</sup> Zhang *et al.* also

found that the *T<sub>c</sub>* of the metal–insulator transition process decreases with a value of ~18 °C for N-incorporated VO<sub>2</sub> thin films, and the narrowing of the charge doping results in the attenuation of the interaction within the V–V dimer in the M1 phase.<sup>18</sup> Dai *et al.* reported that 2.93% F-doped VO<sub>2</sub> foil exhibits an increased solar-heat shielding ability (35.1%), excellent solar modulation ability (10.7%) and appropriate visible transmittance (48.7%).<sup>19</sup> On the other hand, the incorporation of electrons in the VO<sub>2</sub> lattice could also induce its metal–insulator transition.<sup>20–22</sup> For example, NH<sub>3</sub> can act as a reductant to inhibit the over-oxidation of VO<sub>2</sub>, resulting in inferior thermochromic properties.<sup>20</sup> Boron at the interstitial site provides three electrons, and thus, boron doping of VO<sub>2</sub> could drastically reduce the *T<sub>c</sub>* at a rate as large as 31.5 °C per at% B.<sup>21</sup> According to recent theoretical predictions, *T<sub>c</sub>* can be reduced by 27 K per at% W at the GGA+U level or by 18.6 K per at% W at the HSE06 level, which is attributed to W-doping providing three electrons and inducing a large structural distortion in the lattice.<sup>22</sup> Actually, the electron or hole-injection in VO<sub>2</sub> is implemented through these concrete methods such as the doping of N, B, F and other metals. For instance, from the point view of the semiconductor doping process, the W atom has one more valence electron than the V atom, so one W atom substituting for a V atom in VO<sub>2</sub> injects only one additional electron into the compound, whereas a B atom which possess two valence electrons in the 2s orbital at an interstitial site can inject its two 2s electrons into the VO<sub>2</sub>. In addition, the N is widely considered to be the most promising p-type dopant due to its similar size to oxygen, resistance to forming AX centers.<sup>18</sup> The F atom leads to the loss of the V<sup>4+</sup>–V<sup>4+</sup> pairs, as electrons from the donors are injected into the V-3d valence band, resulting in the formation of V<sup>4+</sup>–V<sup>3+</sup> pairs *via* charge transfer.<sup>19</sup> Experimentally, Andreev *et al.* observed that hydrogen atoms penetrated into the VO<sub>2</sub> film during thermal decomposition could lead to a lowered phase transition temperature.<sup>23</sup>

<sup>a</sup>School of Mathematics and Physics, Hubei Polytechnic University, Huangshi 435003, China

<sup>b</sup>School of Materials Science and Engineering, Shanghai University, Shanghai 200444, China. E-mail: [yfgao@shu.edu.cn](mailto:yfgao@shu.edu.cn)

<sup>c</sup>Faculty of Chemical Engineering, Huaiyin Institute of Technology, Jiangsu 223003, China



The above experimental and theoretical results indicate that the  $T_c$  and phase transition behavior of  $\text{VO}_2$  can be effectively controlled by charge doping. However, the role of type of charge on the reduced phase transition temperature is still a debate and remains to be settled. Therefore, it is of vital importance to reveal the underlying mechanism on the effects of charge-doping on the phase transition behavior for realizing the rational tuning of the phase transition temperature.

## 2. Computational details

The calculations were conducted with the Vienna *ab initio* simulation package (VASP).<sup>24,25</sup> The potentials were of the projector augmented wave type (PAW) type, and the exchange-correlation part of the density functional was treated within the generalized gradient approximation (GGA) of Perdew–Burke–Ernzerhof (PBE).<sup>26,27</sup> Given the strong on-site Coulomb repulsion among the V-3d electrons, the Hubbard parameter  $U$  was added to the PBE functional.<sup>28</sup> As discussed in ref. 9 and 10 the value was chosen as 3.4 eV in the PBE+ $U$  formalism. The valence electron configurations for V (3d<sup>3</sup>4s<sup>2</sup>) and O (2s<sup>2</sup>2p<sup>4</sup>) atoms were used in the calculations. 530 eV was used as the plane-wave cut-off energy. The Brillouin zone sampling mesh parameters for the  $k$ -point set were chosen as 5 × 5 × 5 for the electronic structures. These parameters were used to ensure a total energy converges of 1 × 10<sup>-5</sup> eV per unit cell and a maximum force of 0.01 eV Å<sup>-1</sup>. The charge density was tuned by changing the total number of electrons in the unit cell, with a compensating jellium background of opposite charge added or subtracted.<sup>29</sup>

The formation enthalpy of pristine or charge-doped  $\text{VO}_2$  was calculated as

$$\Delta H_f = E_{\text{tot}}(\text{VO}_2) - E_V(\text{bulk}) - 2E\left(\frac{1}{2}\text{O}_2\right) \quad (1)$$

where  $\Delta H_f$  is the formation enthalpy of pristine or charge-doped  $\text{VO}_2$ .  $E_V$  (bulk) is the chemical potential of V in the bulk phase.  $E\left(\frac{1}{2}\text{O}_2\right)$  is the total energy of the oxygen molecules.

The phase transition temperature ( $T_c$ ) can be quantitatively calculated *via*<sup>30</sup>

$$T_c = T_{c,0} \frac{\Delta H}{\Delta H_0} \quad (2)$$

where  $T_{c,0}$  is the transition temperature of pure  $\text{VO}_2$  and a value of 340 K is adopted from ref. 2.  $\Delta H$  and  $\Delta H_0$  are the enthalpy changes associated with the phase transition for doped and pure  $\text{VO}_2$ , respectively. The enthalpy is approximated as the Helmholtz free energy, which can be obtained from our DFT calculations by neglecting the  $pV$  term for condensed matter and omitting the entropy contribution at 0 K.

As shown in Fig. 1(a and b), the basic calculations were performed in the supercells with 2 × 2 × 2 and 2 × 2 × 4 primitive unit cells for  $\text{VO}_2(\text{M})$  and  $\text{VO}_2(\text{R})$  phases, respectively. Table 1 lists the calculated structural parameters. The theoretical lattice parameters obtained in this work are in good agreement with the previously reported experimental data.<sup>31</sup>

## 3. Results and discussion

### 3.1 Charge induced phase transition for $\text{VO}_2$

Fig. 2(a and b) shows the total energies ( $E_{\text{tot}}$ ) of charge doping in M and R phase as a function of charge density. It can be found that the total energies of charge-doping M phase  $\text{VO}_2$  are gradually lower than those of R phase as the charge doping increases, indicating that it is more difficult to obtain R phase  $\text{VO}_2$  than the M phase under current conditions. The similar results have been also appeared in electron-injection in two-dimensional transition metal dichalcogenides.<sup>32</sup> Fig. 2(c and d) shows the formation enthalpy of charge-doped  $\text{VO}_2$ . The trend of the formation enthalpy of electron doping and that of hole doping are contrary. The formation enthalpy of  $\text{VO}_2$  linearly increased with the increase in electron density, while the formation enthalpy of  $\text{VO}_2$  decreased with the increase in hole density. In addition, hole doping system is more negative than the pristine one, and the electron doping system is less negative than the pristine one, suggesting that hole doping system is more stable than the electron doping. Thus, we conclude that

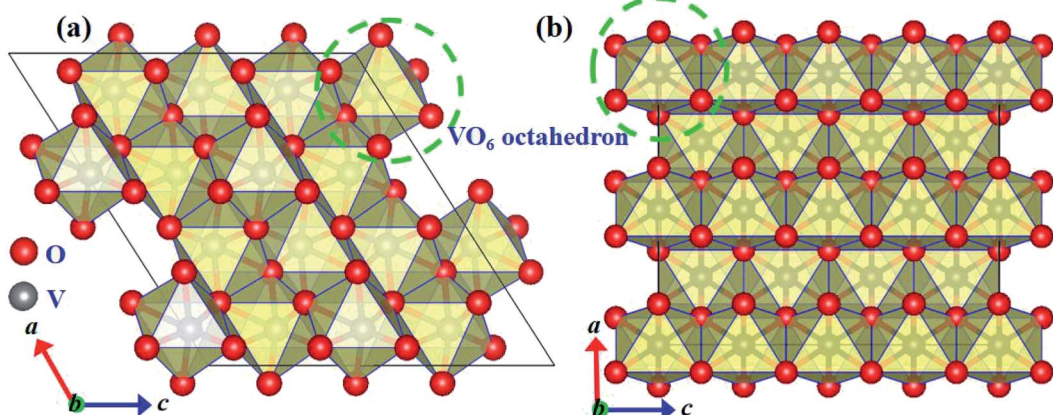


Fig. 1 Crystalline structures of monoclinic (a) and rutile (b) phases of  $\text{VO}_2$ . V and O atoms are represented by gray and red spheres, respectively.



Table 1 Lattice parameters of pristine  $\text{VO}_2(\text{M})$  and  $\text{VO}_2(\text{R})$ 

Systems	$a$ (Å)	$b$ (Å)	$c$ (Å)	$\alpha$ (°)	$\beta$ (°)	$\gamma$ (°)	$V$ (Å $^3$ )	Ref.
$\text{VO}_2(\text{M})$	5.743	4.517	5.375	90	122.6	90	117.466	Exp. <sup>31</sup>
$\text{VO}_2(\text{M})$	5.626	4.637	5.454	90	121.704	90	121.021	This calc.
$\text{VO}_2(\text{R})$	4.552	4.552	2.852	90	90	90	59.095	Exp. <sup>31</sup>
$\text{VO}_2(\text{R})$	4.652	4.652	2.789	90	90	90	60.336	This calc.

hole doping is more conducive to stabilize the structure of  $\text{VO}_2$  than electron doping. This phenomenon has been found in IIA element doping of  $\text{VO}_2(\text{M})$ .<sup>9</sup> Zhang *et al.* reported that the introduction of some electrons in  $\text{VO}_2$  via W doping results in the instability of the structure.<sup>22</sup>

The dependence of  $T_c$  on the charge doping concentration is presented in Fig. 3(a and b). As shown in Fig. 3(a), the  $T_c$  of  $\text{VO}_2$  is found to be almost linearly proportional to the hole-doping density. It is clearly shown that when the hole density is set at  $4.28 \times 10^{21} \text{ cm}^{-3}$ , the phase transition of  $\text{VO}_2$  could take place at 162.44 K, which is lower than the room temperature of 298 K. This observation is consistent with the experimental observation that hole doping could trigger the MIT below 340 K.<sup>17</sup> Wan *et al.* reported that the reduced phase transition temperature for hole doped  $\text{VO}_2$  is due to the fact that hole doping modifies the V-3d orbital occupancy and thus weakens the electron-electron correlation, lowering the crystalline stability energy.<sup>17</sup> Dai *et al.* found that F-doping can effectively decrease the  $T_c$  to 35 °C at 2.93% F in  $\text{VO}_2$  and that F-doping  $\text{VO}_2$  smart glass foils exhibit

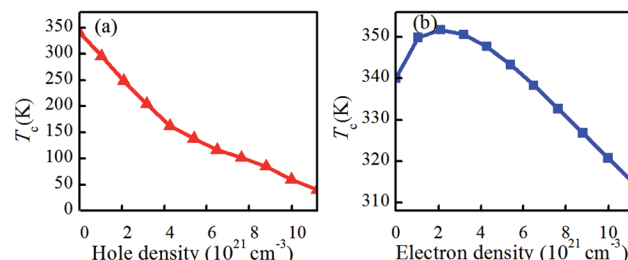


Fig. 3 Dependence of the phase transition temperature ( $T_c$ ) in  $\text{VO}_2$  on the charge density. (a) Hole-doping, and (b) electron doping.

excellent thermochromism in the near-infrared region.<sup>19</sup> However, the situation for electron-doping is not the same as that of hole-doping. As shown in Fig. 3(b), when the electron density increases from 0 to  $2.1 \times 10^{21} \text{ cm}^{-3}$ ,  $T_c$  gradually increases. However, once the electron density is greater than  $2.1 \times 10^{21} \text{ cm}^{-3}$ ,  $T_c$  rapidly decreases. For example, an electron density of  $2.1 \times 10^{21} \text{ cm}^{-3}$  corresponds to a  $\Delta T_c$  of 11.72 K for electron-doped  $\text{VO}_2$ , *i.e.*, the phase transition from the rutile phase to the monoclinic phase occurs at 351.72 K. However, an electron density of  $1.12 \times 10^{22} \text{ cm}^{-3}$  will result in a  $\Delta T_c$  as large as  $-25.32$  K, implying the reduction in  $T_c$  to 314.68 K. Actually, the  $T_c$  is related with the charge concentration. In the range of charge concentration, the  $T_c$  is almost linearly proportional to the charge density. Experimentally, when cooled down to 120 K,  $\text{H}_x\text{VO}_2$  ( $x > 4\%$ ) films exhibit metallic properties, and the  $\Delta T_c$  was around  $-55$  K per at% H.<sup>23</sup>

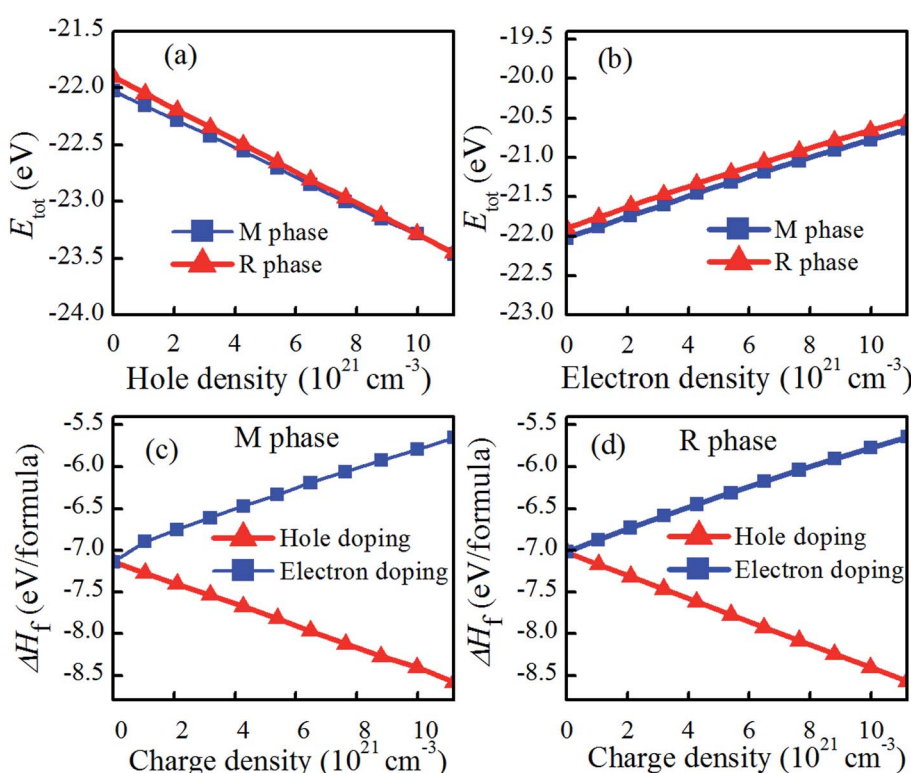


Fig. 2 Total energies ( $E_{\text{tot}}$ ) of charge doping in M and R phase as a function of charge density, and formation energy of charge doped  $\text{VO}_2$ . (a) Hole doping, (b) electron doping, (c) charge doped  $\text{VO}_2(\text{M})$ , and (d) charge doped  $\text{VO}_2(\text{R})$ .



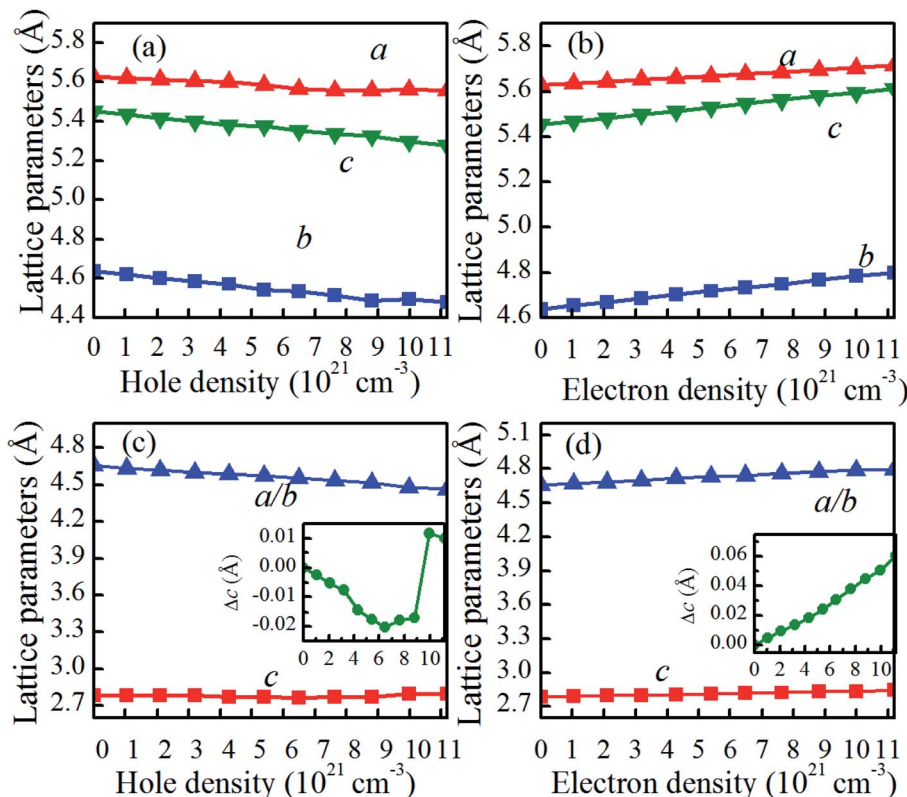


Fig. 4 Lattice parameters of (a) hole or (b) electron doped  $\text{VO}_2(\text{M})$ , and (c) hole or (d) electron doped  $\text{VO}_2(\text{R})$ . The inset figure is the variation of  $c$ , i.e.,  $\Delta c$  ( $c - c_0$ ). The  $c$  and  $c_0$  are the supercell lengths along the  $c$ -axis at equilibrium and charge-doped  $\text{VO}_2$ .

### 3.2 Atomic and electronic structures of charge-doped $\text{VO}_2$

The reduction in  $T_c$  for charge-doped  $\text{VO}_2$  should be coupled with the changes in the atomic and electronic structure, as discussed in the next section. For charge-doped  $\text{VO}_2(\text{M})$ , as shown in Fig. 4(a and b), the lattice parameters  $b$  and  $c$  of are slightly increase, and the lattice parameter  $a$  remains nearly unchanged under the considered electron density. However, these parameters ( $a$ ,  $b$ ,  $c$ ) slightly decrease with increasing of hole density. This outcome further confirms that the reduction in the  $T_c$  in hole doped  $\text{VO}_2$  is due to the shorter  $a$ -axis length.<sup>33,34</sup> Moreover, the lattice parameter  $a$  expressing the V–V chains promotes the transition from the monoclinic phase to the rutile phase at a lower temperature than that of pristine  $\text{VO}_2$ . Applying the compression strain along the  $a$ -axis balances the V–V distance. In addition, applying the compression strain along the  $a$ -axis results in the overlapping of d orbitals, which increases the d bandwidth and then forces it to transition from the monoclinic phase to the rutile phase, thus causing the reduction in  $T_c$ . Experimentally, Fan *et al.* reported that stretching of  $a$ -axis will increase the  $T_c$  of  $\text{VO}_2$  films.<sup>33</sup> Muraoka *et al.* found that the appearance strain along the  $a$ -axis from  $\text{VO}_2/\text{TiO}_2$  thin films has a large influence on the MIT of  $\text{VO}_2$ .<sup>34</sup> Therefore, hole doping in the concentration range considered is able to promote the phase transition in  $\text{VO}_2$ . The opposite is true for electron doping. For charge-doped  $\text{VO}_2(\text{R})$ , as shown in Fig. 4(c and d), the  $c$  axis is slightly shorten, and then slightly elongated in the hole-doping  $\text{VO}_2(\text{R})$ , while the  $c$  axis is slightly

elongated in electron-doping  $\text{VO}_2(\text{R})$ . This may attribute the fact that the charge-injection would induce variable orbital occupancy, which is similar to the experimental results.<sup>19</sup>

It is reported that the V–V chains are one of the key characteristics of  $\text{VO}_2$  in determining the atomic and electronic properties at different phases.<sup>35,36</sup> As shown in Fig. 1, in pristine  $\text{VO}_2(\text{R})$ , all the V atoms arrange uniformly along the  $c$  axis with nearest-neighbor V–V distances of 2.788 Å. However, pristine  $\text{VO}_2(\text{M})$  exhibits Peierls distortion in the V–V chains along the  $a$ -axis, in which the short and long V–V bonds (2.520 Å vs. 3.143 Å) are arranged alternately. Compared with those of pristine  $\text{VO}_2(\text{M})$ , as shown in Fig. 5(a and b), the short and long V–V bond distances are nearly unchanged and still maintain the dimerization characteristics after electron doping. However, hole doping results in a gradual shortening of the long V–V bond distances and a gradual elongation of the short V–V bond distances below a critical hole density of  $6.48 \times 10^{21} \text{ cm}^{-3}$ . This phenomenon could also be observed experimentally in the intermediate phase of  $\text{VO}_2(\text{M}2)$ , in which only half of the V atoms are dimerized, while the other half form chains of is equally spaced atoms.<sup>37</sup> Once above the critical hole density, the alternatively short and long V–V bond distances jump, and the equidistant V–V bond distances (2.7–2.8 Å) are similar to the V–V bond length in  $\text{VO}_2(\text{R})$  (as shown in Fig. 5(a)). These results indicate that  $\text{VO}_2$  transits from the monoclinic phase to the rutile phase within the range of a certain hole-doping density. Yuan *et al.* proved that the appearance of this phenomenon is



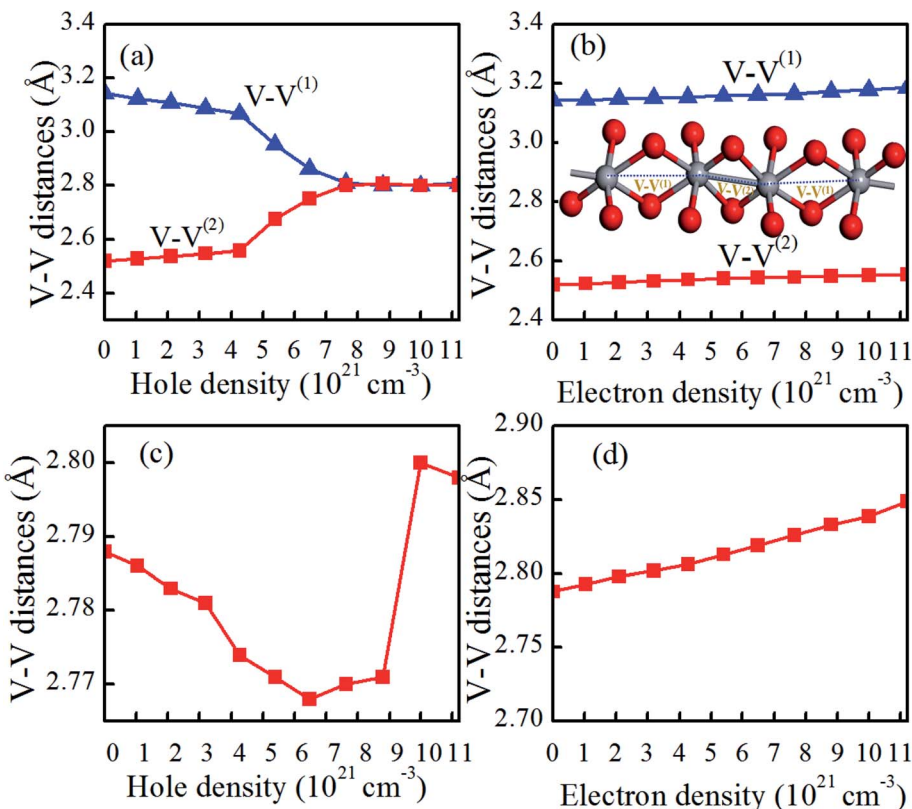


Fig. 5 Dependence of V–V distances in (a) hole or (b) electron doped  $\text{VO}_2(\text{M})$  and (c) hole or (d) electron doped  $\text{VO}_2(\text{R})$  on the charge-doping density. The long V–V bonds denote  $\text{V–V}^{(1)}$ , and the short V–V bonds denote  $\text{V–V}^{(2)}$ . The inserted figure shows the V–V bonds in the  $\text{VO}_2(\text{M})$ . The V and O atoms are indicated by the gray and red spheres, respectively.

attributed to a strong lattice-hole coupling.<sup>38</sup> Experimentally, it is found that a critical hole density induces a sudden rapidly variable V–V bond, which is related to the critical excitation influence.<sup>39–42</sup> As shown in Fig. 5(c), the V–V distances in the hole-doping  $\text{VO}_2(\text{R})$  has a very fast change into alternatively short and long bond distances, for the V–V chains. In contrast, as shown in Fig. 5(d), the V–V distances in electron-doping  $\text{VO}_2(\text{R})$  seem slightly to increase. Therefore, it can be concluded that the hole-injection has greater influence on the V–V bond lengths than the electron-injection in  $\text{VO}_2$ .

The structural transition in  $\text{VO}_2$  is accompanied by changes in the electronic band structure near the Fermi level that can be qualitatively understood within a crystal field model.<sup>31</sup> As shown in Fig. 6(a), the twisting of the V–V chains causes splitting of the  $d_{\parallel}$  orbital into filled bonding and empty antibonding orbitals, while making the  $\pi^*$  orbital move to a higher energy level, thus opening the band gap. Actually, the  $\text{VO}_2$  phase transition is relative to the octahedral environment and the associated hybridization of the O-2p orbitals with the V-3d orbital.<sup>31</sup> As shown in Fig. 6(b), for  $\text{VO}_2(\text{M})$ , each  $\text{VO}_6$  octahedron shares edges with its neighboring octahedra, forming chains along the  $a$ -axis. In addition, the V-3d orbitals split into a combination of low-energy states and high-energy states, where the high-energy states involve the symmetry of the V–O bonds. In charge-doping  $\text{VO}_2(\text{M})$ , as shown in Fig. 6(c and d), the V–O distance is slightly lengthened with the increase in electron density, and could further decrease

the p-d overlap.<sup>43</sup> The increase in the V–O bond results in the expansion of the lattice volume due to the decrease in  $c_{\text{R}}/a_{\text{R}}$  and further induces the reduction in  $T_{\text{c}}$ .<sup>43</sup> Therefore, we can conclude that electron doing makes the V–O bond length longer and thus reduces the  $T_{\text{c}}$  in  $\text{VO}_2$ . However, as the hole density increases, the V–O bond lengths are gradually reduced. When the hole density reaches  $5 \times 10^{21} \text{ cm}^{-3}$ ,  $d_2$  experiences a dramatic increase, and  $d_5$  decreases sharply, which will increase the p-d overlap, and thus both the  $d_{\parallel}$  and  $\pi^*$  orbitals are partially occupied at Fermi level.<sup>43</sup> This phenomenon confirms that  $\text{VO}_2$  may experience a metal-insulator transition.

As shown in Fig. 6(e), in the  $\text{VO}_2(\text{R})$ , the apical and equatorial V–O bond lengths increase with the increase of electron density, which is due to the decrease in the ratio of  $c/a$ . However, as shown in Fig. 6(f), the apical and equatorial V–O bond lengths decrease with the increase hole density.

Except for the variable V–O bond, the band gap evolution of charge-doped  $\text{VO}_2$  is related to the atomic structure change described by the V–V chains and twisting angle  $\delta$  and the electronic structure change described by orbital switching. As shown in Fig. 7(a and b),  $\delta$  in the V–V chains of electron-doped  $\text{VO}_2$  tends to gradually decrease, indicating that the V–V bond characterizes a dimerizing feature. However, when the hole density is from 0 to  $4.28 \times 10^{21} \text{ cm}^{-3}$ ,  $\delta$  in the V–V chains decreases monotonically, as the hole density increase further, the value of  $\delta$  sharply decreases, finally reaching zero, which



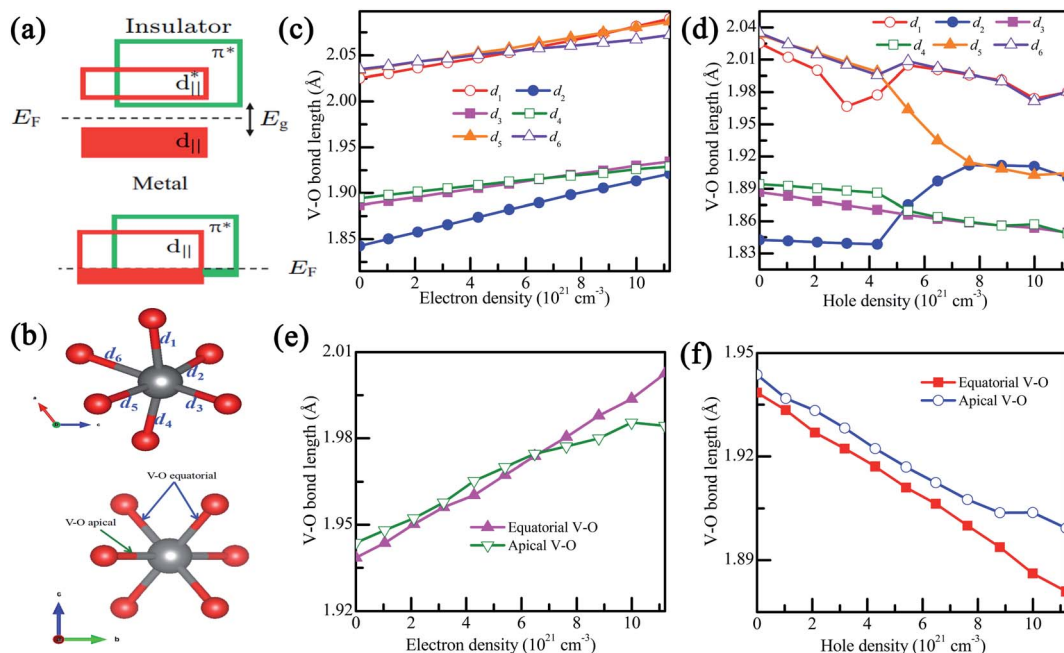


Fig. 6 (a) Bandwidth scheme of pristine  $\text{VO}_2$ , (b) an octahedron at the center of  $\text{VO}_2$ , (c and d) the V-O bond lengths in charge doped  $\text{VO}_2(\text{M})$ , and (e and f) the V-O bond lengths in hole-doped  $\text{VO}_2(\text{R})$ . The bond distances in  $\text{VO}_2(\text{M})$  are  $d_1$ ,  $d_2$ ,  $d_3$ ,  $d_4$ ,  $d_5$  and  $d_6$ . The bond lengths in  $\text{VO}_2(\text{R})$  are the equatorial and apical V-O.

demonstrates that the alternatively short and long V-V bond distances in  $\text{VO}_2(\text{M})$  quickly change into equal V-V bonds. In addition, the average twisting angle  $\delta$  in the V-V chains exhibits

excellent consistency with the band gap change of  $\text{VO}_2$  from R to M1. As in Gao's previous discussion,<sup>35</sup> the significant dimerization in V-V, slight twisting of  $\delta$  or the variable V-O bond can

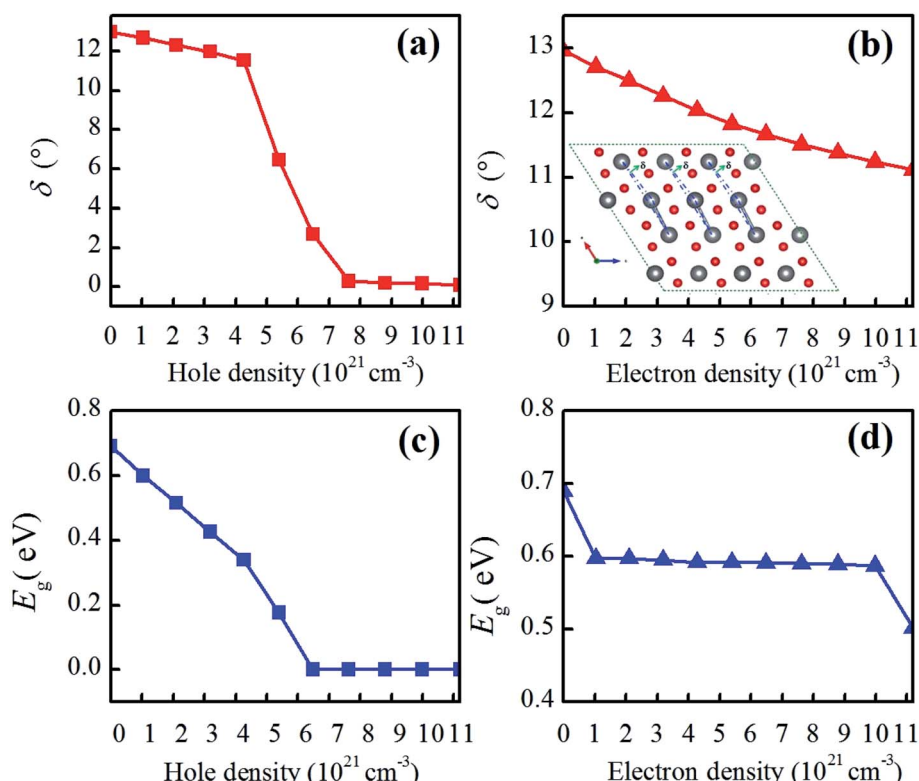


Fig. 7 (a and b) Average twisting angle ( $\delta$ ) of the V-V chains and (c and d) the band gaps in charge-doped  $\text{VO}_2(\text{M})$ . (a and c) Electron doping, and (b and d) hole doping. The inserted figure in (b) is the  $\delta$  angle in the V-V chains in  $\text{VO}_2(\text{M})$ .



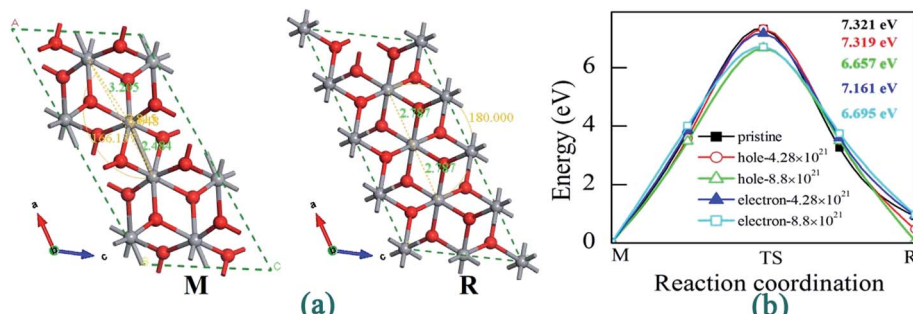


Fig. 8 (a) Structures of VO<sub>2</sub> (M/R) and (b) energy barriers from M to R phase under different charge doping.

be regarded as the characteristic parameters of the structure-driven transition. As shown in Fig. 7(c), when the hole density is increased by  $5.4 \times 10^{21} \text{ cm}^{-3}$ , the band gaps of VO<sub>2</sub>(M) linearly decrease and eventually decrease to 0 eV with the increase in hole density. The band gap undergoes a fast change, and exhibits a similar change tendency as the twisting angle  $\delta$ . This phenomenon is consistent with the other result calculated from Lee *et al.*,<sup>14</sup> who reported that VO<sub>2</sub> exhibits a significant band-gap narrowing for a charge concentration from 0.025 to 0.5 hole/electron per VO<sub>2</sub>. Experimentally, Zhang *et al.* found that N atoms-substituted O atoms induce narrowing of the energy band gap due to weakening of the interaction within the V-V dimer with the hole injected into the  $d_{\parallel}$  sub-bands.<sup>18</sup> In contrast, as shown in Fig. 7(d), as the electron density increases from 0 to  $1.2 \times 10^{22} \text{ cm}^{-3}$ , the band gaps of VO<sub>2</sub>(M) experience a slight reduction ranging from 0.69 eV to 0.502 eV. Apparently, electron doping induces a slow MIT, and its density has some effect on the phase transition. Theoretically, a fascinating rebound behavior of the transition temperature is observed. By increasing the doping concentration of W into VO<sub>2</sub>, the MIT is tuned to a lower temperature at the beginning and then anomalously shifted to a higher temperature.<sup>44</sup>

In order to reveal the kinetic limit for charge-driven phase transition in VO<sub>2</sub>, we performed CINEB calculations to obtain the phase transition barriers. As shown in Fig. 8(a), we redefined the lattice parameters for VO<sub>2</sub>(R) from tetragonal and monoclinic view to better reveal the kinetic limit for charge-driven phase transition in VO<sub>2</sub> (As listed in Table 2). Fig. 8(b) shows the energy curves of M-to-R phase transition in pristine and charge-doping VO<sub>2</sub> with certain density. It can be found that the energy barriers are too higher for VO<sub>2</sub> transiting from M phase to R phase, indicating that it requires additional conditions to

drives the M-to-R phase transition, such as the temperature, pressure and light radiation.<sup>32</sup>

To elucidate the possible driving forces behind the MIT, we further calculated the total and partial densities of states (DOSS) of charge-doped VO<sub>2</sub>(M). As shown in Fig. 9(a), for pristine VO<sub>2</sub>(M), the electrons around  $E_F$  occupy the  $t_{2g}$ -state  $d_{x^2-y^2}$  orbital ( $\pi$ ), while the conduction is mainly occupied by the  $e_g$ -state  $d_{z^2}$  orbital ( $\sigma$ ). At hole densities of  $2.1 \times 10^{21} \text{ cm}^{-3}$  and  $4.28 \times 10^{21} \text{ cm}^{-3}$ , the band gaps of VO<sub>2</sub>(M) are reduced to 0.515 eV and 0.34 eV, respectively. Near the  $E_F$ , the electrons dominantly occupy the  $d_{x^2-y^2}$  orbital and  $d_{yz}$  orbital. In contrast, fewer electrons occupy the  $d_{z^2}$  orbital ( $\sigma$ ). More importantly, this electronic structure characteristic remains from 0 to  $6.48 \times 10^{21} \text{ cm}^{-3}$  (the critical hole density). Interestingly, when the hole density reaches the critical hole density, VO<sub>2</sub> exhibits metallic properties, as shown in Fig. 9(d). There is a strong interaction near the Fermi level between the  $d_{x^2-y^2}$  and  $d_{z^2}$  orbitals. This result is also consistent with the previous discussion on the significant dimerization in V-V and a slight twisting of  $\delta$ , which could be regarded as the characteristic parameters of the structure-driven transition. However, from Fig. 9(e-h), the Fermi levels are shifted into the conduction band to varying degrees with the increase in electron doping. The states near the Fermi level are mainly occupied by the  $d_{z^2}$  orbital, while the valence bands mainly consist of the  $d_{x^2-y^2}$  orbital. Furthermore, it can be observed that the electronic structure of VO<sub>2</sub> changes slightly for different electron concentrations. More importantly, although there are some changes in the band gap from 0.597 eV to 0.502 eV and the location of  $E_F$ , this electronic structure characteristic remains as electron doping increases. Therefore, it can be concluded that the band gap of VO<sub>2</sub> with charge doping should be attributed to an electron-correction-driven Mott transition in which orbital switching occurs between the  $d_{x^2-y^2}$  and  $d_{z^2}$  states. Experimentally, by soft-X-ray absorption spectroscopy, orbital-assisted MIT is also observed in VO<sub>2</sub>.<sup>43</sup>

Fig. 10 shows the density of states of pure VO<sub>2</sub>(R) and charge-doping VO<sub>2</sub>(R). It is seen that pristine VO<sub>2</sub>(R) and charge-doped VO<sub>2</sub>(R) exhibit metallic properties as the Fermi level crosses the conduction band. Furthermore, electrons around Fermi level mainly occupy the  $d_{x^2-y^2}$  orbital and  $d_{z^2}$  orbital. In addition, as the hole density increases, the former has a higher occupant than the latter. However, as the electron density increases, the occupant of  $d_{z^2}$  orbital is higher than that of the  $d_{x^2-y^2}$  orbital. In

Table 2 Calculated lattice parameters for VO<sub>2</sub> (M/R)

VO <sub>2</sub>	$a$ (Å)	$b$ (Å)	$c$ (Å)	$\alpha$ (deg)	$\beta$ (deg)	$\gamma$ (deg)	Ref.
R	4.609	4.609	2.785	90	90	90	35
Monoclinic	5.575	4.653	5.427	90	120.936	90	This calc.
R							
M	5.610	4.571	5.393	90	121.9	90	35
M	5.648	4.634	5.450	90	121.64	90	This calc.



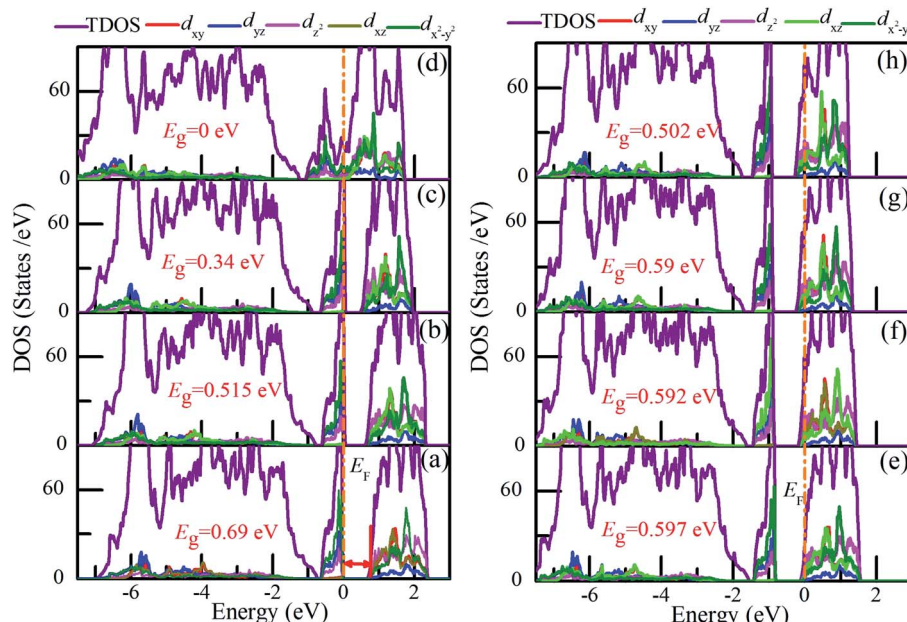


Fig. 9 Total and projected density of states (DOS) of (b-d) hole-doped and (e-h) electron-doped  $\text{VO}_2(\text{M})$ . The concentrations of charge are (a) pristine, (b)  $2.1 \times 10^{21} \text{ cm}^{-3}$ , (c)  $4.28 \times 10^{21} \text{ cm}^{-3}$ , (d)  $8.8 \times 10^{21} \text{ cm}^{-3}$ , (e)  $1.04 \times 10^{21} \text{ cm}^{-3}$ , (f)  $4.28 \times 10^{21} \text{ cm}^{-3}$ , (g)  $7.63 \times 10^{21} \text{ cm}^{-3}$ , and (h)  $1.12 \times 10^{22} \text{ cm}^{-3}$ . The Fermi level ( $E_F$ ) is set to 0 eV.

general, there is a significant orbital switching between the  $d_{x^2-y^2}$  and  $d_{z^2}$  orbitals accompanied by obvious V-V dimerization and a slight twisting of  $\delta$  in the charge-doped  $\text{VO}_2$ .

### 3.3 Discussion

Charge-doping greatly impacts on the atomic and electronic structures of  $\text{VO}_2$ . From the Fig. 3, it is found that the charge-doping including hole and electron-doping could trigger the

phase transition of  $\text{VO}_2$ . More interestingly, the effect of hole doping on the  $T_c$  is greater than that of electron-doping. This is consistent with other calculation result. As is predicted by Zhang *et al.*, the hole doping was superior to electron doping for modulating the phase transition of  $\text{VO}_2$ .<sup>38</sup> From a geometric viewpoint, the octahedra in  $\text{VO}_2$  are orthorhombically distorted, making it possible to differentiate the V-O bonds. After electron-doping, the V-O bond length change significantly in

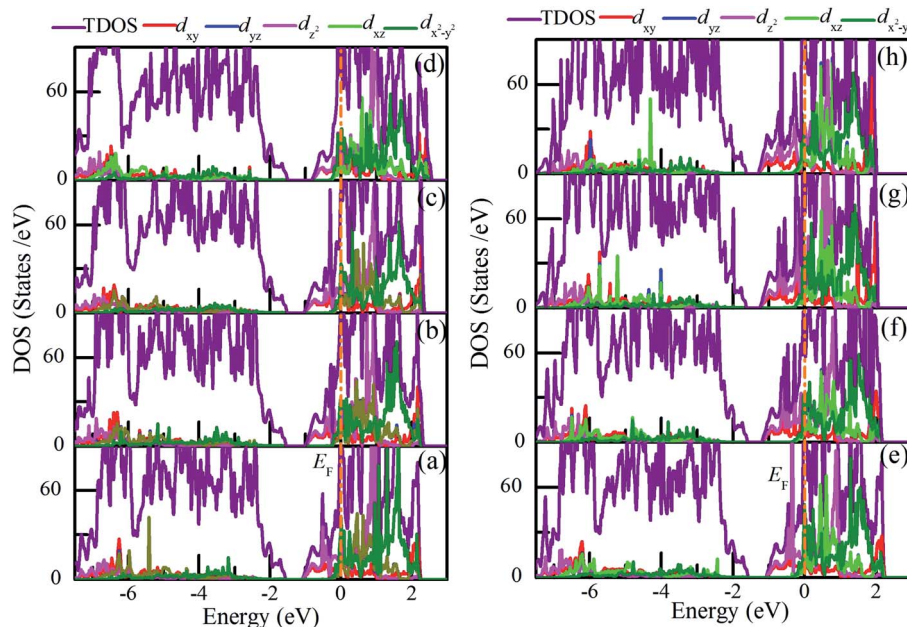


Fig. 10 Total and projected density of states (DOS) of (b-d) hole-doped and (e-h) electron-doped  $\text{VO}_2(\text{R})$ . The concentrations of charge are (a) pristine, (b)  $2.1 \times 10^{21} \text{ cm}^{-3}$ , (c)  $4.28 \times 10^{21} \text{ cm}^{-3}$ , (d)  $8.8 \times 10^{21} \text{ cm}^{-3}$ , (e)  $1.04 \times 10^{21} \text{ cm}^{-3}$ , (f)  $4.28 \times 10^{21} \text{ cm}^{-3}$ , (g)  $7.63 \times 10^{21} \text{ cm}^{-3}$ , and (h)  $1.12 \times 10^{22} \text{ cm}^{-3}$ . The Fermi level ( $E_F$ ) is set to 0 eV.



$\text{VO}_2(\text{R})$ . However, for hole-doping, the alternatively short and long V-V bond distances has very fast change into the equidistant V-V bond in  $\text{VO}_2(\text{M})$ . Furthermore, the twisting angle  $\delta$  experiences a great change. These phenomena are ascribed to structure-driven transition due to the large  $\delta$  and V-V bond length change.<sup>35</sup> From the electronic structure viewpoint, the characteristic of  $\text{VO}_2$  transition from the semiconducting state to the metallic state appears due to the strong interaction between the  $d_{x^2-y^2}$  and  $d_{z^2}$  orbitals near the Fermi level, which can be attributed to the electron-driven the transition. Therefore, it can be concluded that charge-doping may provide an efficient way to modulate the MIT in  $\text{VO}_2$ .

## 4. Conclusions

In summary, we performed first-principles calculations to investigate the behavior of charge doping and its influence on the phase transition temperature of  $\text{VO}_2$ . Charge doping could effectively modulate the  $T_c$ , assisting the  $\text{VO}_2$  phase transition at room temperature. Hole doping induces a significant band-gap narrowing with increasing of hole concentration. The characteristic  $\text{VO}_2$  transition from the semiconducting state to the metallic state appears once above the critical hole density ( $6.48 \times 10^{21} \text{ cm}^{-3}$ ), which is due to the strong interaction between the  $d_{x^2-y^2}$  and  $d_{z^2}$  orbitals near the Fermi level. However, electron doping shows a slight band-gap narrowing with increasing electron concentration. The V-O bond lengths significantly increase. The results will provide insights into phase transitions of  $\text{VO}_2$  thermochromic materials across the MIT suitable for applications such as smart windows.

## Conflicts of interest

There are no conflicts to declare.

## Acknowledgements

The authors gratefully acknowledge support from the National Natural Science Foundation of China (51873102, 51972206), the Open Project Fund of Key Laboratory for Optoelectronics and Communication of Jiangxi Province (20181OEC001), the School-level Scientific Research Project of Hubei Polytechnic University (18xjz11R), and the Innovation Training Program of Hubei Province (S201910920031). The computation was conducted using the high performance computing platform of Shanghai University.

## References

- 1 F. J. Morin, *Phys. Rev. Lett.*, 1959, **3**, 34–36.
- 2 C. Granqvist, *Phys. Scr.*, 1985, **32**, 401–407.
- 3 T. Driscoll, H. Kim, B. Chae, M. Ventra and D. Basov, *Appl. Phys. Lett.*, 2009, **95**, 043503.
- 4 B. Kim, Y. Lee, B. Chae, S. Yun, S. Oh, H. Kim and Y. Lim, *Appl. Phys. Lett.*, 2007, **90**, 023515.
- 5 L. Kang, Y. Gao, H. Luo, J. Wang, B. Zhu, Z. Zhang, J. Du, M. Kanehira and Y. Zhang, *Sol. Energy Mater. Sol. Cells*, 2011, **95**, 3189–3194.
- 6 Y. Gao, S. Wang, H. Luo, L. Dai, C. Cao, Y. Liu, Z. Chen and M. Kanehira, *Energy Environ. Sci.*, 2012, **5**, 6104–6110.
- 7 Y. Cui, Y. Ke, C. Liu, Z. Chen, N. Wang, L. Zhang, Y. Zhou, S. Wang, Y. Gao and Y. Long, *Joule*, 2018, **2**, 1707–1746.
- 8 C. Tang, P. Georgopoulos, M. E. Fine, J. B. Cohen, M. Nygren, G. S. Knapp and A. Aldred, *Phys. Rev. B: Condens. Matter Mater. Phys.*, 1985, **31**, 1000–1011.
- 9 L. Chen, Y. Liu, K. Yang, P. Lan, Y. Cui, H. Luo, B. Liu and Y. Gao, *Comput. Mater. Sci.*, 2019, **161**, 415–421.
- 10 L. Chen, Y. Cui, S. Shi, B. Liu, H. Luo and Y. Gao, *RSC Adv.*, 2016, **6**, 86872.
- 11 S. Zhang, I. S. Kim and L. J. Lauhon, *Nano Lett.*, 2011, **11**, 1443–1447.
- 12 J. P. Pouget, H. Launois, J. P. D'haenens, P. Merenda and T. M. Rice, *Phys. Rev. Lett.*, 1975, **35**, 873–875.
- 13 J. Jeong, N. Aetukuri, T. Graf, T. D. Schladt, M. G. Samant and S. S. P. Parkin, *Science*, 2013, **339**, 1402–1405.
- 14 D. Lee, B. Chung, Y. Shi, G. Y. Kim, N. Campbell, F. Xue, K. Song, S. Choi, J. Podkaminer, T. Kim, P. Ryan, J. Kim, T. Paudel, J. Kang, J. Spinuzzi, D. Tenne, E. Tsymbal, M. Rzchowski, L. Chen, J. Lee and C. Eom, *Science*, 2018, **362**, 1037.
- 15 J. Zhang, H. He, Y. Xie and B. Pan, *Phys. Chem. Chem. Phys.*, 2013, **15**, 4687.
- 16 K. Wang, W. Zhang, L. Liu, P. Guo, Y. Yao, C. Wang, C. Zou, Y. Yang, G. Zhang and F. Xu, *Appl. Surf. Sci.*, 2018, **447**, 347–354.
- 17 M. Wan, M. Xiong, N. Li, B. Liu, S. Wang, W. Ching and X. Zhao, *Appl. Surf. Sci.*, 2017, **410**, 363–372.
- 18 W. Zhang, K. Wang, L. Fan, L. Liu, P. Guo, C. Zou, J. Wang, H. Qian, K. Ibrahim, W. Yan, F. Xu and Z. Wu, *J. Phys. Chem. C*, 2014, **118**, 12837–12844.
- 19 L. Dai, S. Chen, J. Liu, Y. Gao, J. Zhou, Z. Chen, C. Cao, H. Luo and M. Kanehira, *Phys. Chem. Chem. Phys.*, 2013, **15**, 11723–11729.
- 20 M. Wan, B. Liu, S. Wang, L. Hu, H. Tao and X. Zhao, *J. Alloys Compd.*, 2017, **706**, 289–296.
- 21 T. Hajlaoui, N. Émond, C. Quirouette, B. L. Drogoff, J. Margot and M. Chaker, *Scr. Mater.*, 2020, **177**, 32–37.
- 22 J. Zhang, H. He, Y. Xie and B. Pan, *J. Chem. Phys.*, 2013, **138**, 114705.
- 23 V. Andreev, V. M. Kapralova and V. Klimov, *Phys. Solid State*, 2007, **49**, 2318–2322.
- 24 G. Kresse and J. Hafner, *Phys. Rev. B: Condens. Matter Mater. Phys.*, 1993, **47**, 558–561.
- 25 G. Kresse and J. Furthmüller, *Phys. Rev. B: Condens. Matter Mater. Phys.*, 1996, **54**, 11169–11186.
- 26 J. P. Perdew, K. Burke and M. Ernzerhof, *Phys. Rev. Lett.*, 1996, **77**, 3865–3868.
- 27 P. E. Blochl, *Phys. Rev. B: Condens. Matter Mater. Phys.*, 1994, **50**, 17953–17979.
- 28 S. L. Dudarev, G. A. Botton, S. Y. Savrasov, C. J. Humphreys and A. P. Sutton, *Phys. Rev. B: Condens. Matter Mater. Phys.*, 1998, **57**, 1505–1509.



29 L. Chen, A. Wang, Z. Xiong, S. Shi and Y. Gao, *Appl. Surf. Sci.*, 2019, **467–468**, 22–29.

30 M. Netsianda, P. E. Ngoepe, C. Richard, A. Catlow and S. M. Woodley, *Chem. Mater.*, 2008, **20**, 1764–1772.

31 J. Goodenough, *J. Solid State Chem.*, 1971, **3**, 490–500.

32 X. Zhou, H. Shu, Q. Li, P. Liang, D. Cao and X. Chen, *J. Mater. Chem. C*, 2020, **8**, 4432–4440.

33 L. Fan, S. Chen, G. Liao, Y. Chen, H. Ren and C. Zou, *J. Phys.: Condens. Matter*, 2016, **28**, 255002.

34 Y. Muraoka, Y. Ueda and Z. Hiroi, *J. Phys. Chem. Solids*, 2002, **63**, 965–967.

35 S. Chen, J. Liu, H. Luo and Y. Gao, *J. Phys. Chem. Lett.*, 2015, **6**, 3650–3656.

36 T. Yao, X. Zhang, Z. Sun, S. Liu, Y. Huang, Y. Xie, C. Wu, X. Yuan, W. Zhang, Z. Wu, G. Pan, F. Hu, L. Wu, Q. Liu and S. Wei, *Phys. Rev. Lett.*, 2010, **105**, 226405.

37 Y. Ji, Y. Zhang, M. Gao, Z. Yuan, Y. Xia, C. Jin, B. Tao, C. Chen, Q. Jia and Y. Lin, *Sci. Rep.*, 2014, **4**, 4854.

38 X. Yuan, W. Zhang and P. Zhang, *Phys. Rev. B: Condens. Matter Mater. Phys.*, 2013, **88**, 035119.

39 C. Kübler, H. Ehrke, R. Huber, R. Lopez, A. Halabica, R. F. Haglund and A. Leitenstorfer, *Phys. Rev. Lett.*, 2007, **99**, 116401.

40 P. Baum, D. S. Yang and A. H. Zewail, *Science*, 2007, **318**, 788.

41 S. Wall, D. Wegkamp, L. Foglia, K. Appavoo, J. Nag, R. F. Haglund, J. Stähler and M. Wolf, *Nat. Commun.*, 2012, **3**, 721.

42 D. Hilton, R. Prasankumar, S. Fourmaux, A. Cavalleri, D. Brassard, M. Khakani, J. Kieffer, A. Taylor and R. Averitt, *Phys. Rev. Lett.*, 2007, **99**, 226401.

43 N. Aetukuri, A. Gray, M. Drouard, M. Cossale, L. Gao, A. Reid, R. Kukreja, H. Ohladag, C. Jenkins, E. Arenholz, K. Roche, H. Dürr, M. Samant and S. Parkin, *Nat. Phys.*, 2013, **9**, 661–666.

44 M. Nisar, Z. Lin, G. Xu, Y. Liu and G. Han, *J. Appl. Phys.*, 2019, **126**, 195106.

